crystals

Article

Multiple-Layer Triangular Defects in 4H-SiC Homoepitaxial Films Grown by Chemical Vapor Deposition

Yicheng Pei [1,2], Weilong Yuan [1,2], Ning Guo [2,3], Yunkai Li [2,3], Xiuhai Zhang [1,*] and Xingfang Liu [2,3,4,*]

[1] School of Resources, Environment and Materials, Guangxi University, Nanning 530004, China
[2] Key Laboratory of Semiconductor Materials Science, Institute of Semiconductors, Chinese Academy of Sciences, Beijing 100083, China; guoning@semi.ac.cn (N.G.); liyunkai@semi.ac.cn (Y.L.)
[3] College of Materials Science and Opto-Electronic Technology, University of Chinese Academy of Sciences, Beijing 100049, China
[4] Beijing Key Laboratory of Low Dimensional Semiconductor Materials and Devices, Beijing 100083, China
* Correspondence: xiuhaizhang@gxu.edu.cn (X.Z.); liuxf@semi.ac.cn (X.L.)

Abstract: In this study, a special triangular defect (TD) was identified on 4H-SiC epitaxial wafers. The morphology and composition characteristics of these special TDs were revealed by Raman, atomic force microscope (AFM), and scanning electron microscope (SEM). Compared to ordinary triangular defects, this defect protruded from the epitaxial layer and exhibited a laminated shape. The study also discussed the effects of several factors, such as C/Si ratio and growth time, on the triangular defects. Through analysis of these results, we developed methods to suppress the triangular defects. This research provides new insights into the morphology, structure, and composition of this serious destructive defect and is helpful for improving the performance of SiC epitaxial wafers.

Keywords: silicon carbide; extension; triangular defect

Citation: Pei, Y.; Yuan, W.; Guo, N.; Li, Y.; Zhang, X.; Liu, X. Multiple-Layer Triangular Defects in 4H-SiC Homoepitaxial Films Grown by Chemical Vapor Deposition. *Crystals* **2023**, *13*, 1056. https://doi.org/10.3390/cryst13071056

Academic Editor: Evgeniy N. Mokhov

Received: 8 June 2023
Revised: 27 June 2023
Accepted: 2 July 2023
Published: 4 July 2023

Copyright: © 2023 by the authors. Licensee MDPI, Basel, Switzerland. This article is an open access article distributed under the terms and conditions of the Creative Commons Attribution (CC BY) license (https://creativecommons.org/licenses/by/4.0/).

1. Introduction

As a semiconductor material, silicon carbide (SiC) has several advantages over traditional semiconductor materials, including a wide band gap, high thermal conductivity, high critical breakdown field, and high drift velocity of saturated electrons. [1–4]. Consequently, it has become an important material for high-voltage and high-power devices [5–7]. Moreover, 4H-SiC has a larger displacement threshold energy than Si, which makes it resistant to irradiation and high temperature. A major application of 4H-SiC is radiation detection in various fields of applications such as nuclear reactors, cosmic radiation, etc. [8–10].

In recent years, 4H-SiC chemical vapor deposition (CVD) technology has rapidly developed with the breakthrough of key technologies such as "step flow epitaxy" [11,12] and "chlorine-based high-speed epitaxy" [13,14], resulting in gradual improvements in the crystal quality of SiC epitaxial layers. However, the crystal quality still needs to be improved for many high-voltage and high-power SiC power electronic devices. The primary reason for this is the existence of various defects on SiC epitaxial layers, which are often related to factors such as substrate quality, growth temperature, cavity structure, and the crystal structure of the defects [15]. Defects in the active area of high-voltage and high-power SiC electronic devices can cause device failure or performance degradation [16,17]. Therefore, reducing the defect density of epitaxial layers, especially defects with high hazard, is one of the main problems to be solved in 4H-SiC epitaxial growth.

Epitaxial defects in 4H-SiC epitaxial materials can be classified into two categories: crystal defects and surface defects. Crystal defects, also known as structural defects, mainly include point defects, line defects, and surface defects. Point defects consist of impurity atoms, vacancies, interstitial atoms, and their complexes. Line defects include micropipe (MP) and various dislocations, such as threading screw dislocations (TSD), threading edge dislocations (TED), and basal plane dislocations (BPD). Surface defects mainly include

stacking faults (SF). During the epitaxy process, lattice imperfections, foreign particles, substrate surface damage, or process disturbance at the growth interface can lead to the local step flow growth mode change which may introduce surface defects. Surface morphological defects mainly include triangle defects (TDs), carrot defects, downfall, and particles. It is generally believed that microtubules, basal plane dislocations, and surface morphological defects in crystal defects have a greater influence on the performance of devices. Among them, triangular defects are the most destructive surface morphology defects [18].

During our experiments, special triangular defects were found. As shown in Figure 1, they are like ordinary TDs when observed under an optical microscope. However, this special triangular defect has a morphology that resembles an aggregate of TDs and comet-shaped defects. In addition to the characteristics of TDs, its edges are more like the tail of comet-shaped defects. Furthermore, a large portion of these TDs exhibit characteristics similar to comet defect or other defects in the triangular region of TDs [19].

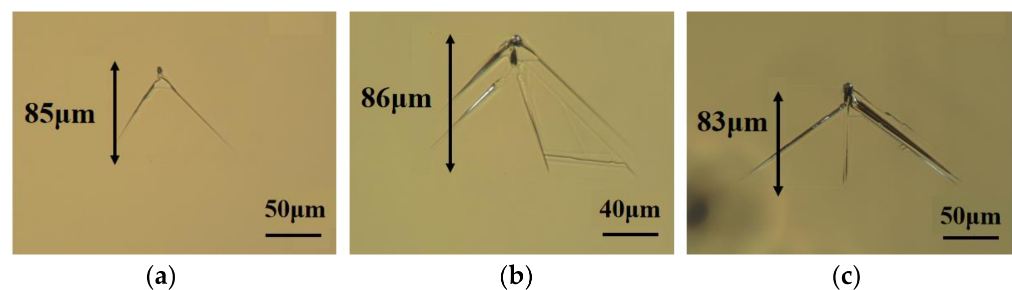

Figure 1. Triangular Defects Photographs under optical microscope. (**a**) Classic Triangular Defects; (**b**,**c**) Special Triangular Defects.

The projection length L of these surface morphological defects like TDs along the [11–20] direction satisfies the equation:

$$L \leq d/\tan\theta, \quad (1)$$

where d is the epitaxial layer thickness and θ is the inclination angle.

This equation shows that the length of surface defects is related to inclination and thickness. At present, 4H-SiC epitaxial wafers are generally grown on substrates with 4° off-angle. Therefore, the thicker the thickness is, the longer the surface morphology defects will be.

On the harmfulness of TDs to devices, TDs are fatal surface morphological defects that increase the reverse leakage current and reduce the breakdown voltage. TDs mostly nucleate at the junction of the epitaxial layer and substrate and extend to the surface of the epitaxial layer. TDs are composed of triangular regions and heads and obtain their name from the overall shape of TDs, which are like triangles. The surface morphology of TDs contains two edges. The triangular head sometimes has an obvious small triangular dent or falling object, and the triangular area in the defect is depressed downward [20].

The special TDs discovered are more likely to be shown as Figure 2 in the following study. The most important feature of these TDs is that they have a multiple-layer structure. The study of multiple-layer structures on other materials provides a theoretical approach to the study of this triangular defect and elucidates the causes of the defect [21,22].

Regarding the structure of traditional TDs, some studies suggest that they are composed of two basal plane dislocations, and stacking faults are involved in the structure of some TDs. These two basal plane dislocations initiate from the junction of the substrate and the epitaxial layer. Then, they propagate to the surface of the epitaxial layer during growth, forming the left and right boundaries of the triangular defect. The stacking fault, caused by the basal plane dislocation, is located between the two boundaries. Others think that not only the above defects, but also TSD, are involved in the formation of triangle defects [23].

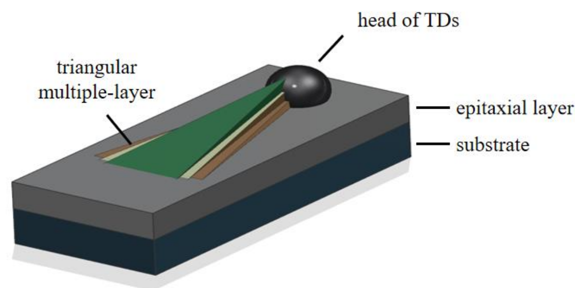

Figure 2. Structural model of special multiple-layer TDs.

On the origin of triangular defects, the classic TDs are closely related to low off-axis (4 or below) epitaxial growth, and the larger step width leads to two-dimensional nucleation on the epitaxial layer [24]. Early research on TDs divided them into two types: those with a core and those without. TDs without a core are generally considered to be caused by differences in growth conditions between the substrate, buffer layer, and epitaxial layer, while TDs with a core are considered to be caused by falling objects or defects of the substrate and nucleation of dislocation (TSD, BPD, MP) [25,26]. In addition, some studies show that collapse in the growth process can lead to the formation of TDs, and some people think that TDs nucleate because of silicon drops falling on the surface [27].

2. Materials and Methods

The experiment was carried out in a horizontal hot-wall chemical vapor deposition equipment. The epitaxy was performed on commercially available 6-inch 4°off-axis 4H-SiC. The growth temperature was set to the temperature of the wafer susceptor, around 1570 °C, and the chamber pressure was controlled at 40 torr. Trichlorosilane (SiH_3Cl, TCS) and ethylene (C_2H_4) were used as the precursors. Hydrogen (H_2) was used as the carrier gas and dilution gas, and the ratio of silicon to H_2 was 0.05%. The initial ratio of carbon to silicon (C/Si) was 1, and the growth time was 30 min, which will be adjusted in later experiments.

The microstructure of defects was observed by SEM, the surface morphology was observed by step meter and AFM, and the composition of defects was determined by a Raman spectrometer.

3. Results

3.1. Composition of Defect

One TD's position and one normal position were taken as Raman test points on three epitaxial wafers with identical growth conditions except for the growth temperatures of 1550 °C, 1570 °C and 1600 °C. Obviously, the Raman peaks of the defect position (the upper three lines) and the ordinary position (the lower three lines) in Figure 3a have completely different performances near the Raman shift around 800 cm^{-1}.

When analyzing the triangular defects and the common positions of epitaxial wafers by Raman spectroscopy, the peak position of 4H-SiC folding longitudinal optics (FLO) at 965.3 cm^{-1} is very close to that of 3C-SiC FLO at 973.5 cm^{-1}, so it is impossible to distinguish between the 4H crystal form and the 3C crystal form. If 3C-SiC is mixed in 4H-SiC, it will be difficult to judge the crystal form. In the process of a Raman measurement, the Raman scattering peak at 798.2 cm^{-1} can be used as a criterion to distinguish between 3C and 4H crystal forms. For 4H-SiC crystal without other crystal inclusions, the relative intensity of folding transverse optics (FTO) scattering peak at 777.0 cm^{-1} is very high, while that at 798.2 cm^{-1} is very small. However, the FTO peak of 3C-SiC is only at 798.2 cm^{-1}, and there are no peaks at 777.0 cm^{-1}. When there are 3C-SiC crystal inclusions in the tested area, the relative intensity of the scattering peak at 798.2 cm^{-1} will increase, and the ratio of the relative intensity of the scattering peaks at 777.0 cm^{-1} and 798.2 cm^{-1} will decrease. Therefore, if the difference between the FTO peak intensity at 777.0 cm^{-1} and

that at 798.2 cm^{-1} is small, it means that 3C-SiC is doped in 4H-SiC, and the content ratio of the mixture of the two crystal forms can also be judged by the peak intensity ratio.

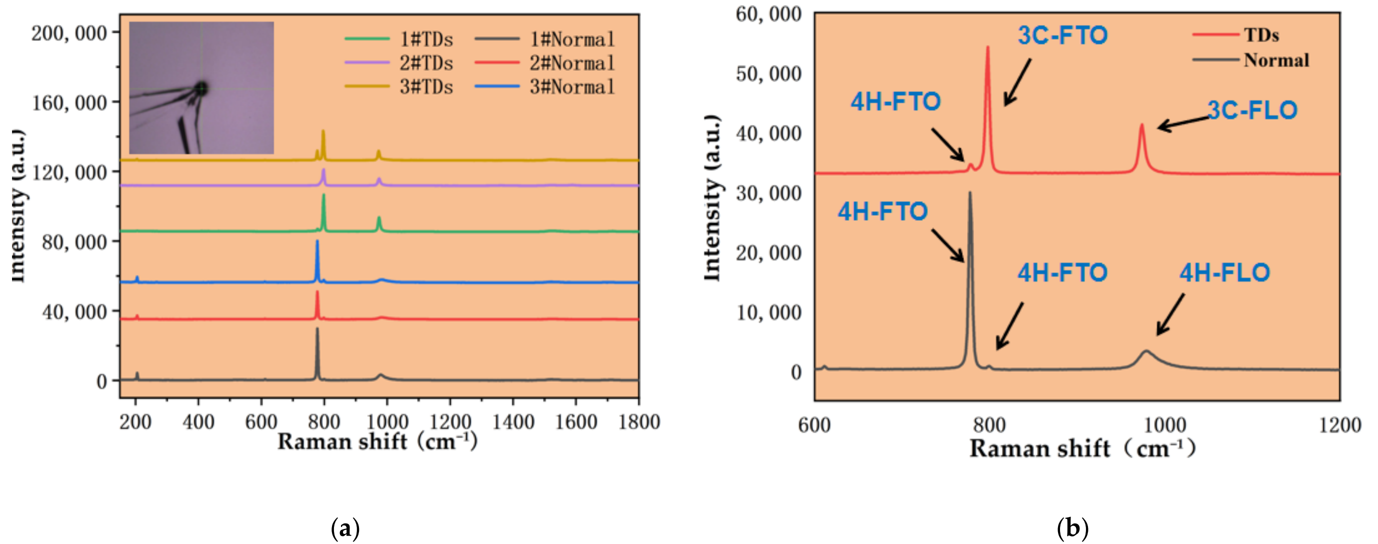

Figure 3. Raman peak diagram of defects on 4HSiC epitaxial wafer. (**a**) comparison of defect positions and common positions of three groups of samples; (**b**) detailed comparison diagrams of defect positions and non-defect positions.

The Raman shift of the defect position on one epitaxial wafer is compared with that of the normal position in detail. As shown in the Figure 3b, the Raman scattering peak in the non-defect area of the black curve meets the Raman shift and peak intensity of 4H-SiC, while the red defect area shows the characteristic peak of 4H-SiC with lower intensity, and the defect area has a characteristic peak of 3C-SiC at 789.2 cm^{-1}, which meets the Raman shift and peak intensity of 3C-SiC. There is a small 4H-SiC FTO peak at 770.0 cm^{-1}, so it can be confirmed that the center of the specific TDs is 3C crystal with a little bit of 4H crystal. Because the 4H-SiC content is very low, it can be considered that the head particle is a polycrystalline particle of 3C-SiC.

3.2. Microstructure

As shown in Figure 4, the epitaxial layer thickness of this batch of epitaxial wafers with triangular defects is approximately 6 μm, and the length of triangular defects is about 80 μm (along the $[11\bar{2}0]$ direction). Two examples were selected for comparison with their morphology under an optical microscope. These examples exhibit similarities in terms of size, opening orientation, and the comet-shaped wake of the boundary. The only noticeable difference is the presence of a smaller head and a central boundary within the triangular defect shown in Figure 4b.

Observation of the morphological characteristics of the triangular defect was conducted under the SEM. The initial impression indicates that the morphology of the defects differs from that of the classical triangular defect. In classical triangular defects, the defect head forms at the junction between the substrate and the epitaxial layer. The two BPDs extend along the 4° off-angle direction to the surface of the epitaxial layer. Due to the presence of these defects hindering the step flow during the epitaxial layer growth process, the step flow will bypass the BPD defects on both sides of the defects. As a result, there is no step flow and epitaxial layer growth behind the triangular defect head, leaving a triangular pit depressed into the epitaxial layer. This is the reason why classical triangular defects have a morphology of depression into epitaxial layers.

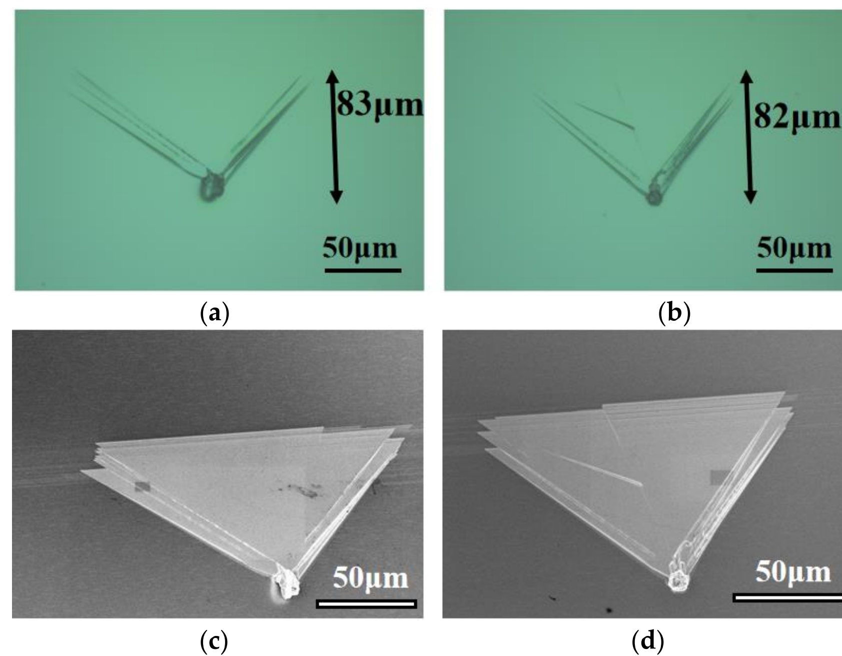

Figure 4. Comparison diagram of triangular defect optical microscope and SEM. (**a**) Defect 1 under optical microscope; (**b**) Defect 2 under optical microscope; (**c**) Defect 1 under SEM; (**d**) Defect 2 under SEM.

However, the specific triangular defect protrudes from the epitaxial layer. In addition, the triangular defect is a multi-layer structure, which has not been reported yet.

The contact position between the defect and the 4H-SiC epitaxial layer is magnified and observed in Figure 5b,c. The step flow is obviously disturbed by the defect. In the area near the defect, the strip steps are very dense. In addition, the defect triangle region still retains the structure of epitaxial layer surface morphology and has dense step morphology. It can be inferred that a large-scale step flow passes through this region but becomes obstructed by the particle. The step flow bypasses the particle on its left and right sides and resumes its progression, only to be captured by the particle and accumulate behind the defect, thus forming a defect layer. Then, several large steps flow through, forming a multi-layer triangular defect structure. The step cluster traces connected with the periphery of the defect on the defect level can be used as evidence of this idea. Moreover, the TDs depicted in Figure 4b,d show that the top two layers have only half triangular defect layers. This may be attributed to the large steps are separated from the particles to the left and right sides. However, steps are not closed after bypassing; the left step is not caught by the particles and continues to move along the flow direction of the steps, while the right step is caught by the particles and lies down to become half defect layers.

The multiple-layer structure is also shown in Figure 5b,c. The upper layer of the triangular area is superimposed on the lower layer. Because the upper layer is slightly longer and narrower, the left and right boundaries of the lower layer become exposed. By the superposition of multiple layers, the left and right boundaries of defects will show the appearance of two comet tails under an optical microscope. In addition, according to the bending direction of the boundary of the layered structure under SEM, the triangular region of the defect protrudes from the surface of the epitaxial layer.

The head of the defect is observed in magnification in Figure 5d. The head of TDs is analyzed by Raman spectroscopy as a 3C crystal different from the epitaxial layer. The particle size of the defect head is about 10 microns, which is embedded in the epitaxial layer. Because some epitaxial wafers are only 6 microns thick, TDs head particles with a diameter of 10 microns still appear. Because most of the special TDs found have large

heads, this research prefers that the defect is caused by falling objects rather than other reasons mentioned in the introduction.

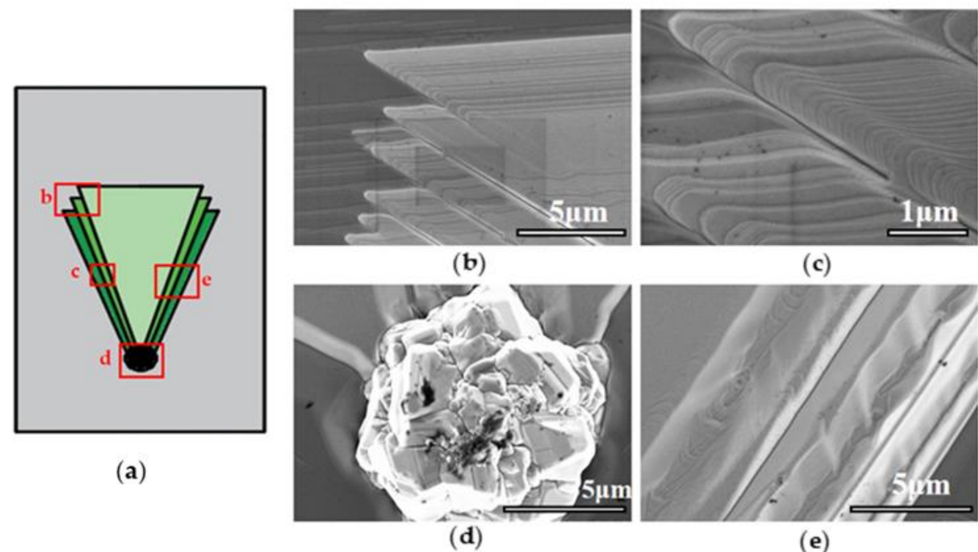

Figure 5. Enlarged detail image of SEM. (**a**) Specific magnification area of SEM; (**b**) The right boundary area of the TD; (**c**) Higher magnification image of the right boundary area, (**d**) The head of TD; (**e**) The right boundary area of TD.

As shown in Figure 6, the cross-sectional image is obtained by the step meter test on the body and the head of the TDs. The cross-sectional image of the triangular area also shows that the triangular defect protrudes out of the epitaxial layer. In addition, the triangular area is not smooth, but rugged, which may be caused by the steps still existing in the triangular area. The cross-sectional size of the head also conforms to the morphology shown by SEM.

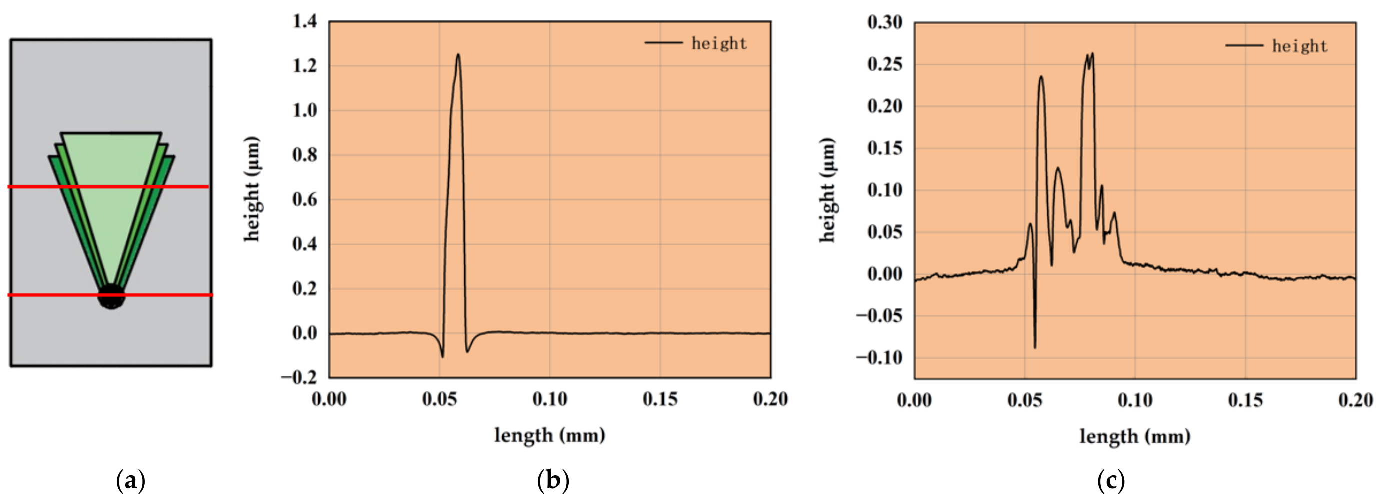

Figure 6. Step meter cross-sectional image of TDs. (**a**) Selection line of sampling position; (**b**) Cross-sectional view of defective body; (**c**) cross-sectional view of defective head.

There is a great difference between the left and right boundaries of TDs in Figure 6. The left boundary can show the stacked shape of multiple defect layers, while the right boundary is particularly steep. In the interface image of the step meter in Figure 7, the left boundary goes deep into the epitaxial layer, while the right boundary reaches the surface of the epitaxial layer.

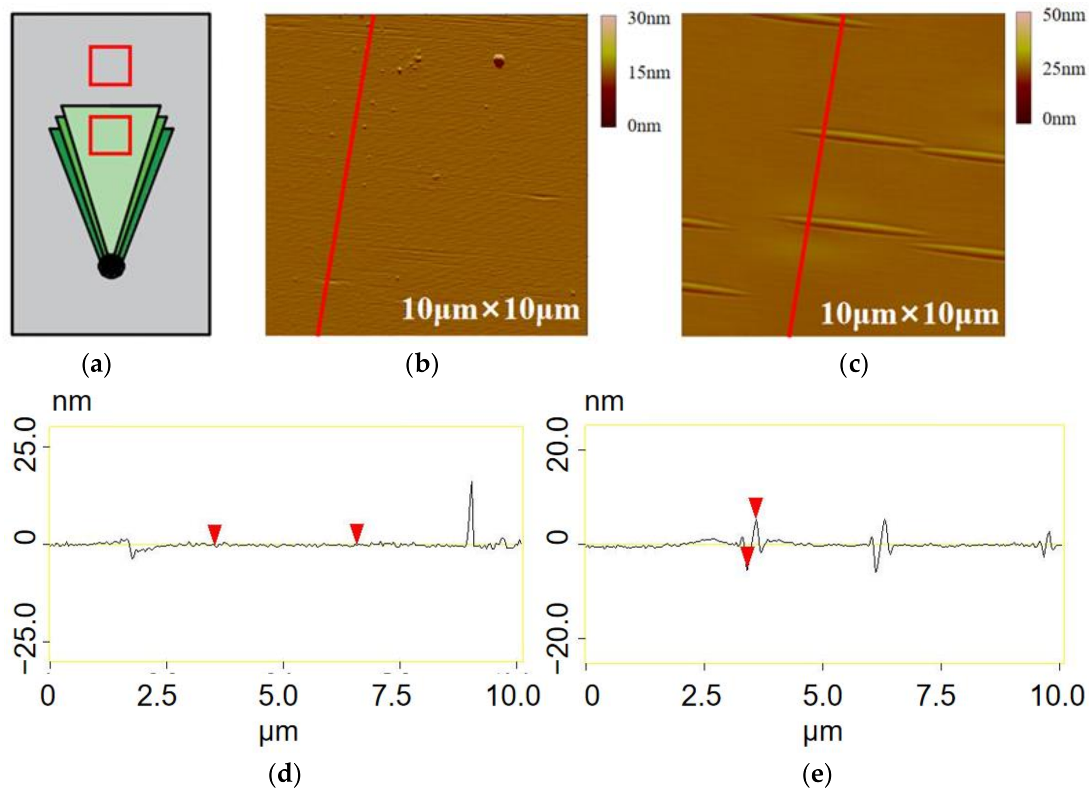

Figure 7. AFM image of different part from the TDs and nearby. (**a**) Test area of AFM; (**b**) AFM image inside the defect; (**c**) AFM image outside the defect; (**d**) Cross-sectional image inside the defect; (**e**) Cross-sectional image outside the defect.

The morphological difference between the triangular surface of the triangular defect and the surface of the epitaxial layer nearby in Figure 6 is compared. On the one hand, the obvious long strip structures are shown outside the defect. The strip structures observed in the figure are uniformly oriented perpendicular to the $[11\bar{2}0]$ crystal direction and parallel to the $(1\bar{1}00)$ crystal plane. The strip shape appears to be a combination of convex peaks and concave valleys in cross-section. However, it consists of two peak–valley structures, resulting in two large height fluctuations on the surface. Along the step flow direction, the first height fluctuation includes a small peak and a large valley, while the second height fluctuation includes a large peak and a small valley. This two connected peak–valley structure is referred to as the "double peak–valley structure" [28], which mainly describes the giant steps on the epitaxial wafer. The width, length, and depth of each strip-shaped morphology in the figure are similar, and the size of the entire strip-shaped morphology can be confirmed by the cross-sectional view obtained through atomic force microscopy. The length of the strip-shaped morphology is about 3 μm; the absolute height from the deepest point to the highest point is approximately 11 nm; and the width is about 300 nm. The stripe morphology increases the roughness of the epitaxial layer surface, which may have an adverse effect on the subsequent device preparation and increase the leakage current of the device.

Because the direction of the whole strip morphology is perpendicular to the direction of step flow and consistent with the direction of step clustering and the bimodal-valley structure is almost consistent with step clustering, it is considered that the strip morphology is related to the step flow of epitaxial growth, which may be caused by the phenomenon of step flow and incomplete step clustering. The epitaxial growth of 4H-SiC is mainly controlled by step flow, and the density of surface atomic steps on the substrate with 4° off-angle is smaller than that on the substrate with 8° off-angle or higher. This makes the surface of the epitaxial layer grown on the substrate with 4° off-angle prone to step

aggregation, and several atomic steps tend to aggregate into a large step after epitaxy. Because the step aggregation is more likely to be formed under carbon-rich conditions, the C/Si used in the experiment is less than or equal to one. The process of step aggregation is not totally completed, but presents a relatively discrete state, thus forming this special strip shape.

On the other hand, the surface inside the defect looks smoother than the outside when there were no strip structures. However, the root mean square roughness of the inside (1.119 nm) is more than that of the outside (0.919 nm), which may because the short steps from the outside still appear inside but are much denser and thinner. Another reason is that there are many small particles on the surface of TDs like the cross-sectional image of Figure 7d.

3.3. *Influence Methods*

Exploring the influence of C/Si ratio, epitaxial growth time, and buffer layer on the number of TDs in epitaxial wafers, the C/Si ratio is changed by changing the ratio of TCS to ethylene, keeping the flux of TCS unchanged, and reducing the flux of ethylene to reduce the C/Si ratio. Statistics of the number and distribution of defects are carried out by photoluminescence detector as in Figure 8.

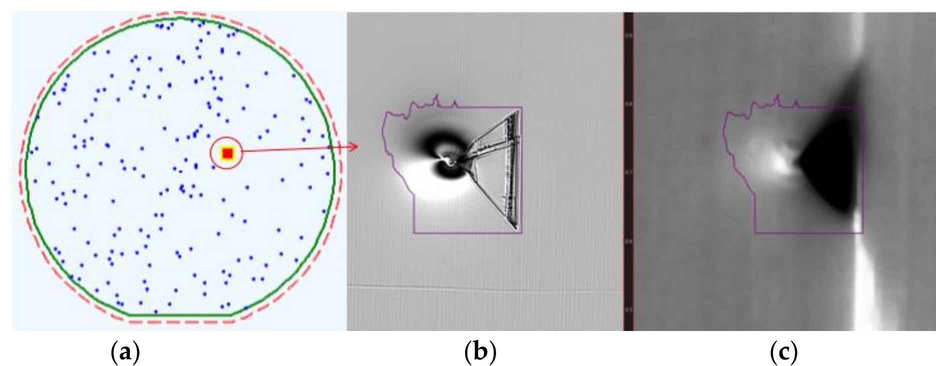

Figure 8. Photoluminescence TDs detection. (**a**) Distribution image of TDs; (**b**) TD under bright field channels; (**c**) TD under photoluminescence channels.

The TCS flux was set at 50 sccm, and the ethylene flux was adjusted at 25 sccm, 20 sccm and 18 sccm, so that the C/Si ratio was 1, 0.8 and 0.72, respectively. Under these conditions, epitaxial growth was carried out for 30 min.

The box diagram in Figure 8, drawn according to the obtained data, shows that the number of special TDs is less under the condition of low carbon. The TDs can be reduced to some extent under the condition of rich silicon, which may be because it is easier to generate clusters of SiC particles at the top of the chamber when the carbon content is higher.

Judging from the curve of TDs average value changing with growth time, the number of defects is not positively correlated with growth time. Too short or too long growth time will lead to a sharp increase in the number of triangle defects, while the number of triangle defects is less when the growth time is 20 to 30 min.

The reason for this phenomenon may be that there are two origins of the triangular defect: one origin is that the defect on the substrate nucleates, and the other reason is that the particles nucleated at the top of the epitaxial furnace fall off. Many TDs in the short-time epitaxy of 10 min are more likely to be caused by the nucleation of defects on the substrate; they are also more likely to be caused by the nucleation and falling of particles at the top during the epitaxy of 40 min. These two factors work together, resulting in a concave curve that falls first and then rises in the growth time of 10–40 min.

Figure 9c evidences that the buffer layer grown on the epitaxial wafer plays a crucial role in determining the outcome of TDs. The buffer layer is grown under specific conditions, including a H_2 flow of 100 slm, TCS flow of 50 sccm, ethylene flow rate of 25 sccm, growth

pressure of 40 Torr, growth temperature of 1570 °C, and growth time of 4 min. Two types of buffer layers were grown during the experiment: one with a nitrogen flow rate of 40 sccm, and the other with a nitrogen flow rate of 300 sccm. The number of TDs decreased significantly after the buffer layer was grown. This is because the buffer layer prevented some substrate defects from extending into the epitaxial layer and transforming into surface morphological defect nucleation points. Moreover, stress and interface defects caused by the difference of doping concentration between the substrate and the epitaxial layer can become the nucleation sites of TDs, which can be suppressed by adding the buffer layer. The difference in the effect of the buffer layer grown with different nitrogen flow rates in Figure 9c is due to the difference in doping concentration.

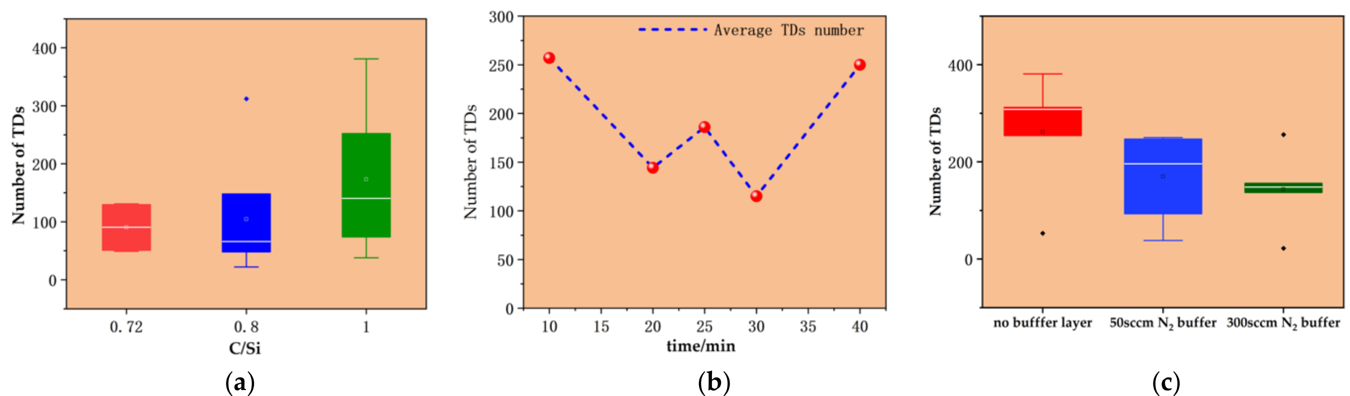

Figure 9. Statistical chart of TDs quantity under the influence of different factors. (**a**) Variation of TDs number under different C/Si ratio; (**b**) Variation of TDs number under different growth time; (**c**) Variation of TDs number under different buffer layer.

4. Discussion

Based on the comprehensive analysis of the morphology of the triangular defect, we can establish a process model of the triangular defect formation.

Firstly, the characteristics of the triangular defect are briefly described: (1) the triangular defect protrudes from the epitaxial layer; (2) there are large particles in the head; (3) the triangular defect is multi-layered; (4) there are similar but denser step clusters on the defect surface.

Let us construct this triangular formation model: (1) epitaxial layer is ready to start growing on the substrate; (2) 3C-SiC particles fall on the substrate or 2D nucleation from substrate defect; (3) epitaxial layer grows and starts step flow; (4) large-scale step flow passes by the particles; a short flight of step was caught and lay behind the particles; (5) the next large-scale step passes by the cluster particles and was caught; (6) repeat (7) special TDs generation.

The next part discusses three factors that affect this special triangle defect: carbon–silicon ratio, growth time, and buffer layer. The main purpose is to find a control method of triangle defect and to explain the formation of this special triangle defect by comparing the causes of triangle defect in the introduction section. In the silicon-rich environment, this special triangle defect is less frequent, which shows that the head particles should not be formed by silicon droplets. The number of triangular defects varies with time, indicating that some triangular defects are born in the epitaxial process; the growth of buffer layer can control triangular defects, which shows that this special triangular defect is also partly caused by substrate defects.

There may be other factors that can reduce the number of defects in the triangle, such as growth temperature and gas flow rate, which are not fully explored in this paper. They can be explored in the future.

5. Conclusions

Our research shows that TDs in the experiment own the following morphological characteristics: protruding from the epitaxial layer; multilayered structure; and surface asperities. It is related to both the substrate defect and the falling objects. The silicon-rich condition, buffer layer, or suitable growth time is more conducive to inhibiting the nucleation of these TDs.

The triangular defect that we found with a new multiple-layer structure protruding from the epitaxial layer further reveals more morphology, structure, and composition of this serious destructive defect. At the same time, we discuss some factors that affect this defect, which is of certain significance to the control of triangular defect. For some defects on silicon carbide epitaxial wafers, the current research still cannot perfectly clarify their destructiveness and defect origin; however, it is hoped that the study of this triangular defect will further improve the properties of silicon carbide epitaxial wafers.

Author Contributions: Methodology, formal analysis, data curation, writing—original draft preparation, Y.P.; Data curation, formal analysis, visualization, W.Y.; Software, supervision, resources, validation, N.G. and Y.L.; Project administration, Investigation, Supervision, X.Z.; Conceptualization, Supervision, Funding acquisition, Writing—review and editing, X.L. All authors have read and agreed to the published version of the manuscript.

Funding: This work was supported by the National Key R&D Program of China (Grant No. 2021YFB3401603) and the National Natural Science Foundation of China (Grant No. 12175236).

Data Availability Statement: The data that support the findings of this study are available from the corresponding author, X.Z. and X.L., upon reasonable request.

Conflicts of Interest: No potential conflict of interest was reported by the authors in this paper.

References

1. Xu, M.; Girish, Y.R.; Rakesh, K.P.; Wu, P.; Manu Kumar, H.M.; Byrappa, S.M.; Udayabhanu; Byrappa, K. Recent advances and challenges in silicon carbide (SiC) ceramic nanoarchitectures and their applications. *Mater. Today Commun.* **2021**, *28*, 102533. [CrossRef]
2. Kaloyeros, A.E.; Goff, J.; Arkles, B. Defect- and H-Free Stoichiometric Silicon Carbide by Thermal CVD from the Single Source Precursor Trisilacyclohexane. *Electron. Mater.* **2022**, *3*, 27–40. [CrossRef]
3. Zhao, Z.; Li, Y.; Xia, X.; Wang, Y.; Zhou, P.; Li, Z. Growth of high-quality 4H-SiC epitaxial layers on 4° off-axis C-face 4H-SiC substrates. *J. Cryst. Growth* **2020**, *531*, 125355. [CrossRef]
4. He, Y.; Yuan, Z.; Song, S.; Gao, X.; Deng, W. Investigation on Material Removal Mechanisms in Photocatalysis-Assisted Chemical Mechanical Polishing of 4H–SiC Wafers. *Int. J. Precis. Eng. Manuf.* **2021**, *22*, 951–963. [CrossRef]
5. Wellmann, P.J. Review of SiC Crystal Growth Technology. *Semicond. Sci. Technol.* **2018**, *33*, 103001. [CrossRef]
6. Matsunami, H. Fundamental research on semiconductor SiC and its applications to power electronics. *Proc. Jpn. Acad. Ser. B-Phys. Biol. Sci.* **2020**, *96*, 235–254. [CrossRef]
7. Dong, L.; Sun, G.S.; Yu, J.; Zheng, L.; Liu, X.F.; Zhang, F.; Yan, G.G.; Li, X.G.; Wang, Z.G.; Yang, F. Characterization of Obtuse Triangular Defects on 4H-SiC 4° off-Axis Epitaxial Wafers. *Chin. Phys. Lett.* **2013**, *30*, 96105. [CrossRef]
8. Chaudhuri, S.; Mandal, K. Radiation Detection Using n-Type 4H-SiC Epitaxial Layer Surface Barrier Detectors. In *Advanced Materials for Radiation Detection*; Springer: Berlin/Heidelberg, Germany, 2022; pp. 183–209. ISBN 978-3-030-76461-6.
9. Napoli, M.D. SiC detectors: A review on the use of silicon carbide as radiation detection material. *Front. Phys.* **2022**, *10*, 769. [CrossRef]
10. Mandal, K.C.; Krishna, R.; Muzykov, P.G.; Laney, Z.; Sudarshan, T.S. Radiation Detectors Based on 4H Semi-Insulating Silicon Carbide. In Proceedings of the International Society for Optics and Photonics, Wuhan, China, 2–5 November 2010; Volume 7805, pp. 158–165.
11. Saitoh, H.; Kimoto, T. 4H-SiC Epitaxial Growth on SiC Substrates with Various Off-Angles. In Proceedings of the Materials Science Forum, Boston, MA, USA, 28 November–2 December 2005; Volume 483, pp. 89–92.
12. Kimoto, T.; Yonezawa, Y. Current status and perspectives of ultrahigh-voltage SiC power devices. *Mater. Sci. Semicond. Process.* **2018**, *78*, 43–56. [CrossRef]
13. Pedersen, H.; Leone, S.; Kordina, O.; Henry, A.; Nishizawa, S.-i.; Koshka, Y.; Janzén, E. Chloride-Based CVD Growth of Silicon Carbide for Electronic Applications. *Chem. Rev.* **2012**, *112*, 2434–2453. [CrossRef]
14. Liu, X.F.; Yan, G.G.; Liu, B.; Shen, Z.W.; Wen, Z.X.; Chen, J.; Zhao, W.S.; Wang, L.; Zhang, F.; Sun, G.S.; et al. Process optimization for homoepitaxial growth of thick 4H-SiC films via hydrogen chloride chemical vapor deposition. *J. Cryst. Growth* **2018**, *504*, 7–12. [CrossRef]

15. La Via, F.; Camarda, M.; La Magna, A. Mechanisms of growth and defect properties of epitaxial SiC. *Appl. Phys. Rev.* **2014**, *1*, 031301. [CrossRef]
16. Fujiwara, H.; Naruoka, H.; Konishi, M.; Hamada, K.; Katsuno, T.; Ishikawa, T.; Watanabe, Y.; Endo, T. Impact of Surface Morphology above Threading Dislocations on Leakage Current in 4H-SiC Diodes. *Appl. Phys. Lett.* **2012**, *101*, 042104. [CrossRef]
17. Taishi, T.; Hoshikawa, T.; Yamatani, M.; Shirasawa, K.; Huang, X.; Uda, S.; Hoshikawa, K. Influence of crystalline defects in Czochralski-grown Si multicrystal on minority carrier lifetime. *J. Cryst. Growth* **2007**, *306*, 452–457. [CrossRef]
18. Zhao, L. Surface defects in 4H-SiC homoepitaxial layers. *Nanotechnol. Precis. Eng.* **2020**, *3*, 229–234. [CrossRef]
19. Hu, J.; Jia, R.; Xin, B.; Peng, B.; Wang, Y.; Zhang, Y. Effect of Low Pressure on Surface Roughness and Morphological Defects of 4H-SiC Epitaxial Layers. *Materials* **2016**, *9*, 743. [CrossRef]
20. Niu, Y.X.; Tang, X.Y.; Jia, R.X.; Sang, L.; Hu, J.C.; Yang, F.; Wu, J.M.; Pan, Y.; Zhang, Y.M. Influence of Triangle Structure Defect on the Carrier Lifetime of the 4H-SiC Ultra-Thick Epilayer. *Chin. Phys. Lett.* **2018**, *35*, 077103. [CrossRef]
21. Kakanakova-Georgieva, A.; Ivanov, I.G.; Suwannaharn, N.; Hsu, C.-W.; Cora, I.; Pécz, B.; Giannazzo, F.; Sangiovanni, D.G.; Gueorguiev, G.K. MOCVD of AlN on epitaxial graphene at extreme temperatures. *CrystEngComm* **2021**, *23*, 385–390. [CrossRef]
22. Sangiovanni, D.G.; Faccio, R.; Gueorguiev, G.K.; Kakanakova-Georgieva, A. Discovering atomistic pathways for supply of metal atoms from methyl-based precursors to graphene surface. *Phys. Chem. Chem. Phys.* **2022**, *25*, 829–837. [CrossRef]
23. Wu, P.; Emorhokpor, E.; Yoganathan, M.; Kerr, T.; Zhang, J.; Romano, E.; Zwieback, I. Dislocation in 4H n^+ SiC Substrates and their Relationship with Epilayer Defects. In Proceedings of the Materials Science Forum, Boston, MA, USA, 26–30 November 2007; Volume 556, pp. 247–250.
24. Matsunami, H.; Kimoto, T. Step-controlled epitaxial growth of SiC: High quality homoepitaxy. *Mater. Sci. Eng. R Rep.* **1997**, *20*, 125–166. [CrossRef]
25. Hallin, C.; Konstantinov, A.O.; Pécz, B.; Kordina, O.; Janzén, E. The origin of 3C polytype inclusions in epitaxial layers of silicon carbide grown by chemical vapour deposition. *Diam. Relat. Mater.* **1997**, *6*, 1297–1300. [CrossRef]
26. Zhao, L.; Wu, H. A correlation study of substrate and epitaxial wafer with 4H-N type silicon carbide. *J. Cryst. Growth* **2019**, *507*, 109–112. [CrossRef]
27. Li, Y.; Zhao, Z.; Yu, L.; Wang, Y.; Zhou, P.; Niu, Y.; Li, Z.; Chen, Y.; Han, P. Reduction of morphological defects in 4H-SiC epitaxial layers. *J. Cryst. Growth* **2019**, *506*, 108–113. [CrossRef]
28. Wang, J.; Zhao, S.; Yan, G.; Shen, Z.; Zhao, W.; Wang, L.; Liu, X. Investigation on Step-Bunched Homoepitaxial Layers Grown on On-Axis 4H-SiC Substrates via Molten KOH Etching. *Crystals* **2022**, *12*, 788. [CrossRef]

Disclaimer/Publisher's Note: The statements, opinions and data contained in all publications are solely those of the individual author(s) and contributor(s) and not of MDPI and/or the editor(s). MDPI and/or the editor(s) disclaim responsibility for any injury to people or property resulting from any ideas, methods, instructions or products referred to in the content.